J. Fluid Mech. (1970), *vol.* 40, *part* 3, *pp.* 549–576
Printed in Great Britain

Thermal instability and convection of a thin fluid layer bounded by a stably stratified region

By J. A. WHITEHEAD† AND M. M. CHEN‡
Yale University, New Haven, Conn.

(Received 18 December 1968 and in revised form 30 September 1969)

Results of linear stability calculations and post-stability experimental observations are reported for horizontal fluid layers with upward heat flux bounded below by a stably stratified fluid. Stability calculations were done for several families of continuous and discontinuous temperature distributions, and it was found that as a rule the flow originating in the unstable layer penetrates into the stably stratified region, resulting in increased critical cell size and correspondingly decreased critical Rayleigh number. A notable exception to this occurs for an unstable layer with a linear temperature distribution adjacent to a stable layer of very high stable density gradient. In this case energy pumped from the unstable to the stable region is sufficient to raise the critical Rayleigh number above that of a solid boundary. It is also found that, for density distributions with a more gradual transition between the stable and the unstable regions, the effect of increased cell size upon the critical Rayleigh number is sometimes masked by effects of curvature in the density profile of the unstable region, which tends to increase the critical Rayleigh number. The inadequacy of the usual definition of Rayleigh number to characterize the stability of such complex systems is discussed. Experimentally, such a temperature distribution was produced by radiant energy from above as it was absorbed by the top few centimetres of the fluid. Within an uncertainty of $\pm 20\%$, it was found that the critical experimental Rayleigh number agreed with neutral stability calculations. The supercritical convective motion consisted of vertical jets of cool surface fluid which plunged downward into the interior of the fluid. The jets were not arranged in an orderly lattice but were in a constant state of change, each jet having a tendency to merge with a close neighbour. The net loss of jets due to merging was balanced by new jets spontaneously appearing. As Rayleigh number was increased, the mean number of jets and the intermittancy increased proportionally. Temperature scans taken with a movable probe showed that cool surface fluid plunging downward in the jets was confined to a fairly restricted region, the surrounding fluid being quite isothermal.

† Present address: Institute of Geophysics and Planetary Physics, University of California, Los Angeles.

‡ Present address: Department of Mechanical Engineering, New York University, New York.

1. Introduction

This communication reports the results of a study of motionless fluid layers with unstable temperature gradients bounded by one or two stably stratified regions, as shown in figure 1. The body of the text has two sections, 2 and 3; § 2 (i) and § 2 (ii) are concerned with the effects of the shape of the density profiles and the magnitude of the adjacent stable gradients upon the stability conditions and the small amplitude flows associated with the corresponding eigenfunctions. Physically interesting temperature distributions of several representative classes are considered. In § 3 (i) and (ii), experimental observations are reported for the stability and qualitative structure of finite amplitude supercritical flow for a family of profiles produced by non-uniformly distributed radiative heating. Parameters of the flow, such as the horizontal length scales and vertical temperature differences, are also shown.

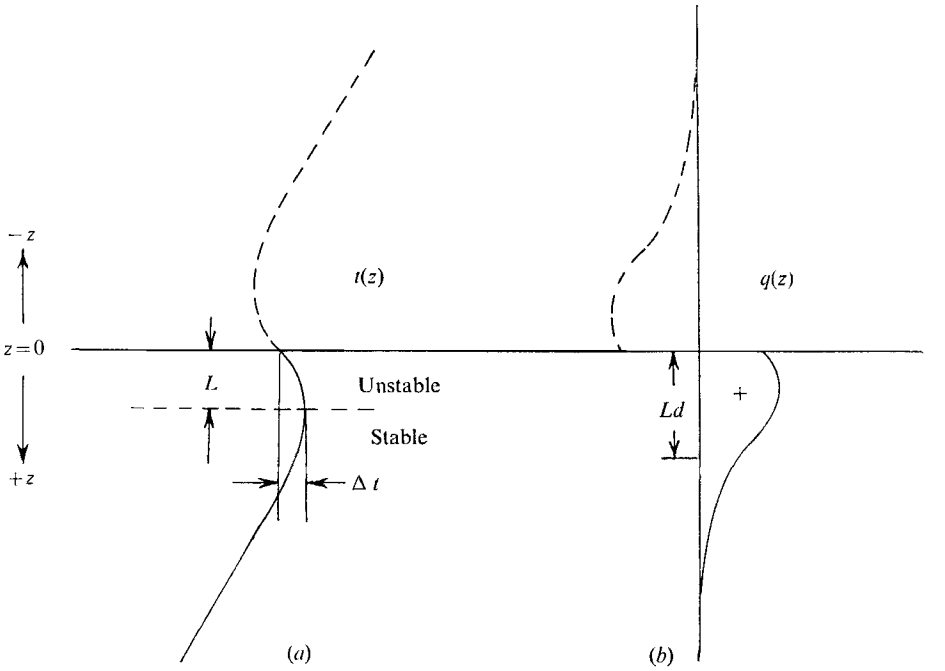

FIGURE 1. Schematic representation of (*a*) a thermally unstable layer bounded by a stably stratified region and (*b*) its generating heat source distribution.

The problem differs from the classical Rayleigh–Bénard problem (see Chandrasekhar 1961, chapter I) in that the perturbations in the unstable region are coupled to flows in the adjacent regions which have stable temperature gradients. Our study is motivated by the realization that thermal instability is a simple prototype of many fluid and plasma problems currently under active study, and that in a large number of these, if not the majority, the relevant adverse gradient is confined to only a limited region of the entire volume being studied.

It is perhaps more obvious that such locally unstable layers are frequently found in the atmosphere and the oceans, as attested by the number of related papers cited below. It should not be difficult to see that equivalent situations are found in the problem of Taylor instability for flows between counter-rotating cylinders, and of particular relevance to the profiles chosen in this study, for flows along concave surfaces where the primary adverse velocity gradient exists in the boundary layer. The closely related interchange instabilities in plasmas almost always originate in thin layers of sharp density or field gradients (Lehnert 1967).

An obvious example of convective flow in nature is the isothermal region near the ocean surface, which in many situations is created by intense but localized mixing due to temporal lowering of the surface temperature. This often occurs in an otherwise stably stratified ocean, the stratified fluid lying below the convecting fluid. Similar situations are found in atmospheres and lakes due to solar heating of the ground and lake bottoms. Although these processes are caused ultimately by transient effects, the disparity between the slow time scale associated with surface changes and the fast time scale associated with convective eddies renders the problem quasistatic.

The volume heating employed in the present experiments is in the form of progressively attenuated radiation from above. One may find direct analogues of this situation in oceanography and meteorology. The importance of volume heating in the topmost few metres of ocean water has been pointed out by Kraus & Rooth (1961). Although they felt that solar heating as a source of the fluid kinetic energy is not as important as wind shear, it can be easily demonstrated with the results of § 3 (i) and (ii) of this paper, that, in the absence of wind, solar heating is more than adequate to produce intense thermal convection. It is also not difficult to see that similar thermal convection due to distributed solar heating may be present in shallow lakes containing turbid waters and on top of smoggy air masses. In the latter case sunlight, absorbed by the topmost layer of the smog, contributes to the temperature reversal in the smog but promotes convective mixture between the smog and the clear air above.

It has already been demostrated that in systems with complex temperature profiles finite amplitude effects may be important even at very low Rayleigh numbers (Veronis 1963; Krishnamurti 1968*a*). Currently available techniques for non-linear analysis (Segel 1967), on the other hand, require *a priori* assumptions concerning the phenomenological nature of the flow, e.g. periodicity, quasi-steadiness, etc. Thus experimental observations are needed as a guide for the theoretical studies.

2. Density profiles and stability conditions

(i) *Stability calculations*

Although the governing equations for the several problems cited above are similar, most of the existing theoretical studies have been motivated by thermal convection problems of geophysical interest. However, because of mathematical convenience rather than physical considerations, these studies are confined to either piecewise linear density profiles or parabolic density profiles. The solutions

of the former (Gribov & Gurevich 1957; Rintel 1967) can be obtained by matching the boundary conditions for separate solutions of each linear region which is governed by well-known equations. These profiles are clearly unrealistic. It is also not immediately clear whether the artificial discontinuities might give rise to anomalous results.

The solution for the parabolic density profile, mathematically equivalent to the Taylor instability of counter-rotating cylinders originally solved by Chandrasekhar (1961, pp. 289–317), has also been solved with various modifications by Veronis (1963) and Krishnamurti (1968*a*, *b*). While the profile is physically meaningful to the three respective physical models which were suggested by the above authors, it is not always relevant in the geophysical contest, where the adjacent stable regions are usually much larger in dimension than the unstable layer, and occasionally have stable gradients much smaller in magnitude than the unstable gradients. Having a constant second derivative, the parabolic density profiles do not lend themselves to the study of the influences of the magnitude of stable gradients.

While these simple distributions are clearly advantageous for analytical studies where qualitative theoretical questions have to be answered, for the quantitative determination of stability conditions (the case of Gribov *et al.* and Rintel), their advantage is marginal. The authors have consequently chosen first to investigate more complex distributions in the interest of answering specific questions related to the shape of the distributions. This necessitated the use of numerical techniques for the integration of the relevant eigenvalue problem; the problem does not appear to have qualitative features subtly different from those considered by Chandrasekhar and Veronis.

The formulation. We shall assume that the profile in question arises when a fluid layer, with thermal expansion coefficient α, is heated internally by a horizontally uniform heat source $Q(z)$. Adopting the Boussinesq approximation, the continuity, momentum and energy equations in dimensionless form are:

$$\nabla . \mathbf{u} = 0, \tag{2.1}$$

$$Pr^{-1}\{(\partial \mathbf{u}/\partial \tau) + Ra(\mathbf{u} . \nabla \mathbf{u})\} = -\nabla p + \nabla^2 \mathbf{u} - t\mathbf{k}, \tag{2.2}$$

$$(\partial t/\partial \tau) + Ra(\mathbf{u} . \nabla t) = \nabla^2 t + Q(z), \tag{2.3}$$

where the dimensionless parameters Ra and Pr are defined as

$$Ra = g\alpha L^3 \Delta \mathscr{t}/\kappa\nu, \tag{2.4}$$

$$Pr = \nu/\kappa. \tag{2.5}$$

In these expressions g is the gravitational constant, κ the thermometric conductivity, ν the kinematic viscosity, t the dimensionless temperature perturbation $(1/\Delta \mathscr{t})\mathscr{t}$, and $\mathbf{u}$ is the dimensionless velocity $(\nu/g\alpha\Delta \mathscr{t} L^3)\mathbf{u}$. Script characters denote dimensional variables.

Contrary to the classical Rayleigh–Bénard problem, there is no longer a clear-cut choice for the characteristic dimension L and the characteristic temperature difference in $\Delta \mathscr{t}$ the above normalization. Some authors (Sparrow, Goldstein & Jonsson 1963; Krishnamurti 1967) chose to retain the conventional definition

and use the total depth between the top and bottom boundaries as L. While this choice is satisfactory when the depth of the stable layer is small relative to the unstable layer, it is clearly unsatisfactory when the depth of the stable layer is large. It becomes completely meaningless for an infinitely deep stable layer when one boundary, isolated by the stratified fluid from the destabilized layer, plays no role whatsoever on the fluid motion.

An alternative choice for L is the length scale L_q of the heat flux function $\mathscr{q}(z)$ (see figure 2). Note that since attention here is focused on temperature profiles with slopes approaching $-\beta$ at large distances, $\mathscr{q}(z)$ must vanish rapidly for z large relative to a certain value, which can then be identified as L_q. An example is a partially transparent fluid layer heated from above by radiation, such as the case investigated experimentally, where L_q represents the extinction length of the radiation field. The advantage of using L_q for a length scale is that it is a given parameter and that it remains a finite constant for infinitely deep stable layers. Unfortunately, L_q is neither equal to nor directly related to the actual depth of the destabilized layer.

Because of these considerations, it was decided to use the destabilized layer depth and its temperature difference as L and $\Delta\mathscr{t}$. Although these two quantities are not directly given, they can be evaluated easily from the motionless solution of the problem, whose determination is not considered central to the instability problem. There is a possibility that convection would change the depth of the temperature maximum, so in reporting the post-critical parameters the L selected was that L found by solving the heat equation with no motion. The value of $\Delta\mathscr{t}$ was the physically measured temperature difference.

Using an overbar to denote the motionless solution and script $\mathscr{t}$, z and $\mathscr{q}$ to denote that they are dimensional, we have

$$(d^2\bar{\mathscr{t}}/dz^2)+\mathscr{q}(z) = 0, \tag{2.6}$$

where $$\mathscr{q}(z) = Q(z)/\kappa,$$

for the boundary conditions,

$$t(0) = t_0, \quad \bar{\mathscr{t}}(0) = \bar{\mathscr{t}}_0 \quad \text{at} \quad z = 0, \tag{2.7}$$

$$(\partial\bar{\mathscr{t}}/\partial z)\rightarrow -\beta \quad \text{as} \quad z\rightarrow\infty. \tag{2.8}$$

The solutions are, implicitly,

$$\beta = \int_L^\infty \mathscr{q}(z)\,dz, \tag{2.9}$$

$$\Delta\mathscr{t} = \int_0^L \left\{-\int_z^0 \mathscr{q}(z')\,dz\right\} dz. \tag{2.10}$$

The perturbation equations. We shall next consider that the unperturbed solution $\bar{\mathbf{u}}$ $(=0)$ and $\bar{t}$ are disturbed by infinitesimal perturbations $\tilde{\mathbf{u}}$ and $\tilde{t}$. Using normal mode techniques in assuming

$$\tilde{\mathbf{u}} = \mathbf{U}(z)\,e^{i(a.x)+\sigma t}, \tag{2.11}$$

$$\tilde{t} = T(z)\,e^{i(a.x)+\sigma t}, \tag{2.12}$$

it can be shown that the amplitude functions $W(z)$ and $T(z)$ obey the following equations:

$$(D^2-a^2-\sigma)\,T = -Raf(z)\,W, \tag{2.13}$$

$$(D^2-a^2-Pr^{-1}\sigma)\,(D^2-a^2)\,W = a^2T, \tag{2.14}$$

where the normalized density gradient

$$f(z) \equiv \partial\bar{t}/\partial z \tag{2.15}$$

is considered known. It approaches $\beta L/\Delta\ell$ as $z\to\infty$.

This problem differs from the classical Rayleigh–Bénard problem primarily as a result of the variable coefficient $f(z)$ on the right-hand side of (2.13). This function is the only link between the linear stability problem and the agency by which the density distribution is produced. Derivations with somewhat similar results have been given by Morton (1957) and Foster (1965*a*).

Analogous to the Rayleigh–Bénard problem, we consider two types of boundary conditions for the top surface:

$$W = D^2W = T = 0, \quad \text{free isothermal boundaries,} \tag{2.16}$$

$$W = DW = T = 0, \quad \text{non-slip isothermal boundaries.} \tag{2.17}$$

Either boundary condition could also be considered for the bottom boundary. Of course, when the stable layer is infinitely deep, all quantities and derivatives must vanish for large z. In this case it is immaterial whether (2.16) or (2.17) is used.

From the foregoing it is clear that the linear stability problem is an eigenvalue problem as stated in (2.13) and (2.14) and one of the two boundary condition sets (2.16) or (2.17). Giving the Rayleigh number Ra and the dimensionless density or temperature profile $\bar{t}(z)$ completely specifies the problem.

An important property of the temperature profile is its asymptotic slope $\beta L/\Delta\ell$. Following Gribov & Gurevich (1957), this property will be stated in terms of the dimensionless parameter S:

$$S = g\alpha\beta L^4/\kappa\nu. \tag{2.18}$$

The choice of this form, rather than simply $\beta L/\Delta\ell$, is inspired by the consideration that S more accurately describes the response of the stably stratified layer to perturbations with length scales of the order of L.

It is to be expected that any influence of the unperturbed density distribution on the results of the linear stability problem must be a functional of $\bar{t}(z)$. Consequently, one cannot describe other relevant properties of the temperature profile by one or two simple parameters. To investigate the influence of the profiles, one must then compare several families of profiles, with individual members of each family characterized by the parameters Ra and S. These families will be described in detail in a later section.

A considerable simplification occurs for all solutions of neutral stability, because it has been shown that a neutral mode is non-oscillatory for free boundaries, that is, $\sigma_i = 0$ when $\sigma_r = 0$ for growth rate $\sigma = \sigma_r + i\sigma_i$. Proofs for the parabolic temperature distributions with free boundaries have been given by

Veronis (1963), modelled after an unpublished proof for arbitrary temperature distributions by Spiegel. The same technique is easily used for any general distribution. An analogous proof for rigid boundaries could not be found, although, since the non-slip boundary only increases dissipation, it is expected that such flows would also be non-oscillatory. For more detail on the proof for free boundaries, interested readers are referred to Whitehead (1968), and for rigid boundaries readers are referred to the heuristic discussions of Chandrasekhar (1961) concerning the exchange of stabilities of the Taylor instability problem.

For non-oscillatory, neutral modes ($\sigma = 0$), (2.13) and (2.14) can be combined to eliminate T, resulting in

$$(D^2 - a^2)^3 W = -Ra\, a^2 f(z)\, W. \tag{2.19}$$

Our task is to solve for the eigenvalue $Ra = Ra(a)$ for a given $f(z)$, subject to appropriate boundary conditions for the top and bottom surfaces. The minimum value of Ra and its corresponding wave-number yields the critical quantities Ra_c and a_c.

Method of solution. Although we are primarily interested in problems with infinitely deep stable layers, the numerical solution can be handled somewhat more conveniently for a finite depth D. The problem is then solved for a dimensionless depth D/L. The asymptotic values of the results for large D/L are taken as the infinite solution.

To facilitate the numerical integration of (2.19), use is made of three auxiliary functions W_j ($j = 1, 2, 3$). These have all six derivatives specified at $z = 0$, such that the top three boundary conditions (2.16) or (2.17) are satisfied, and so that each of the three functions is independent. All solutions of the equation, including those satisfying the bottom ($z = D/L$) boundary conditions, must be linear combinations of W_j:

$$W = AW_1 + BW_2 + CW_3. \tag{2.20}$$

The three unknown constants can be determined by applying the three boundary conditions at the bottom.

In actual computation, a trial value of Ra_c is assumed for a given wave-number a, and the three W_j's are evaluated by stepwise integration of (2.19) using repeated application of series solution around each new value of z. When W_j and their derivatives are evaluated at $z = D/L$, the bottom boundary conditions are utilized to determine the unknowns A, B and C. Since all boundary conditions are homogeneous, there are in fact only two independent unknowns, say B/A and C/A, for the three equations. The compatibility condition for these equations is then used to check whether the trial Ra_c is correct. If the assumed Ra_c is incorrect, the equations would be found to be incompatible, and a new value of Ra_c would be assumed and the process repeated until a solution of satisfactory precision is obtained. Details of the method of calculation are found in Whitehead (1968).

The estimated error for the most unfavourable case (linear–linear profile with $S = 10^6$) is approximately 6×10^{-4}. For the bulk of the computations the error is considerably smaller.

Temperature profiles. Calculations have been carried out for three simple

families of temperature profiles. It is instructive to consider them as consequences of the limiting forms of the heat source function $Q(z)$.

The simplest case arises when the heat source is not well-distributed, but is concentrated in the vicinity of a particular depth. In that limit, $Q(z)$ is represented by the delta function

$$Q(z) = \kappa\{\beta + (\Delta t/L)\}\,\delta(z - L). \tag{2.21}$$

The resulting temperature profile is then linear in the two intervals $(0, L)$, (L, D) with a discontinuity in slope at $z = L$ (see figure 2(*a*)). This is the profile considered by Gribov & Gurevich (1957) and Rintell (1967). We shall refer to this as the linear–linear profile.

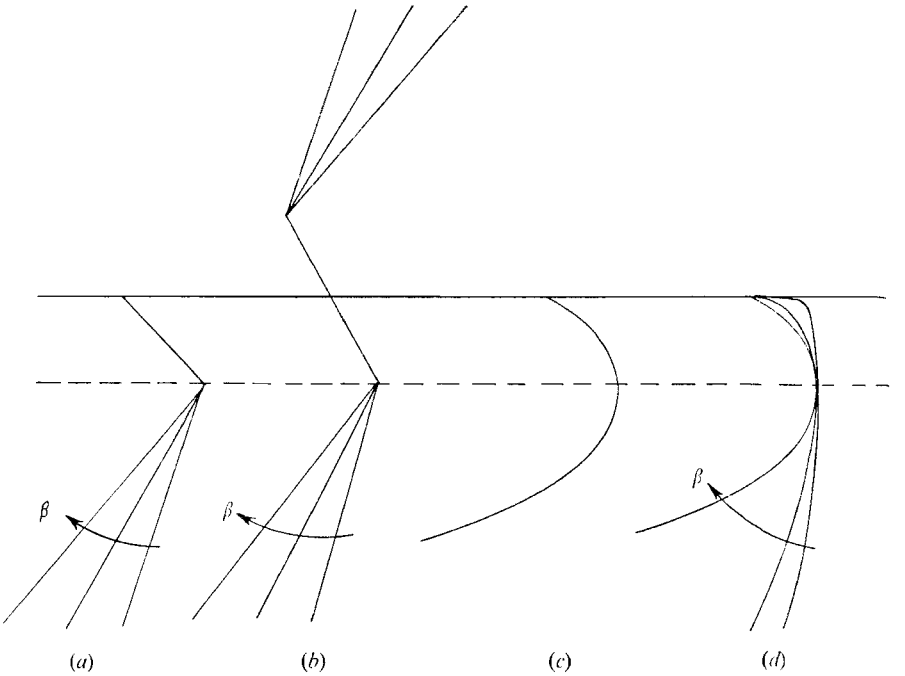

FIGURE 2. The four temperature distributions $\bar{t}(z)$ whose stability was investigated in this work.

A special case of this is a temperature profile which is antisymmetric about the origin (figure 2(*b*)) where no solid boundary is assumed to exist. This profile will be referred to as the linear-antisymmetric profile. It is obtained numerically by noting that the temperature is antisymmetric about the plane $z = 0$, and $f(z)$ is correspondingly symmetric. This causes (2.19) to be symmetric about $z = 0$, in which case $DW = D^3W = D^5W = 0$ at $z = 0$. The antisymmetrical results are thus obtained by using these as boundary conditions at $z = 0$.

Both these profiles are rather artificial and unlikely to be found either in nature or in the laboratory.

At the opposite extreme $Q(z)$ could be such a slowly varying function that its length scale L_q could be considerably greater than L. This occurs when the conditions are such that the major portion of the heat flux flows downward into the

stably stratified region. If $Q(z)$ is non-zero at the origin and remains relatively constant over a depth greater than L, the temperature profiles could be assumed to be parabolic (figure 2(*c*) and (*d*)). This is the problem analyzed by Veronis (1963). It should be noted that for the parabolic profile the temperature gradient approaches infinity as depth approaches infinity. Therefore S is not a freely varying parameter in such a situation.

One of the simplest and most physically meaningful profiles permitting an assignable stable gradient S is the one arising out of an exponential heat source function

$$Q(z) = c \exp[-z/z_0], \tag{2.22}$$

which could conceivably be the result of unidirectional radiation absorbed by a grey fluid, where $1/z_0$ can be identified with the volume absorption coefficient. z_0 may also be identified with the L_q discussed above. When this heat source is present in a fluid layer which has an asymptotic stabilizing gradient β, the following profile is produced (figure 2(*d*)):

$$\ell = -\xi e^{-z/z_0} - \beta z. \tag{2.23}$$

Note that, as a consequence of our definition of L, the latter is a variable depending on β, z_0 and ξ. From (2.9) and (2.10),

$$L = z_0 \ln(\xi/\beta z_0), \tag{2.24}$$

$$\Delta\ell = \xi - \beta z_0(\ln(\beta z_0/\xi) - 1). \tag{2.25}$$

This family of profiles shall be referred to as the 'exponential-linear profile'. It is seen that, for $\beta z_0/\xi \gg 1$, the profile approaches the parabolic profile in the most important upper portions.

(ii) *Discussion of results*

Piecewise-linear distributions. The results for piecewise-linear distributions are shown in figures 3–5.

Influence of stratified layer depth. The variation of critical Rayleigh number and critical wave-number with D/L is shown in figure 3. It is seen that, except for very large S, both Ra_c and a_c decrease with increasing depth for small depths, and approach a constant asymptotic value for large depths. Examination of these figures indicates that the decrease in critical Rayleigh number was in a large part due to the increase of convection cell size, which is proportional to the reciprocal of the critical wave-number. In the limit of large depth, the cell size becomes a function of S only, with the consequence that Ra_c approaches an asymptotic value for a given S. The following discussions are concerned with these asymptotic values of Ra_c and a_c.

The influence of stabilizing gradient as $S \to 0$. The dependence of Ra_c and a_c on S for the linear–linear distribution with an infinitely deep stable region is shown in figure 4. It is seen that for low values of S, both Ra_c and a_c decrease with decreasing S. This is a manifestation of the fact that for low values of S, the cell size is not limited by the unstable depth L, but by the inherent depth scale associated with the decay of perturbations in the stably stratified region, a quantity which increases with decreasing S.

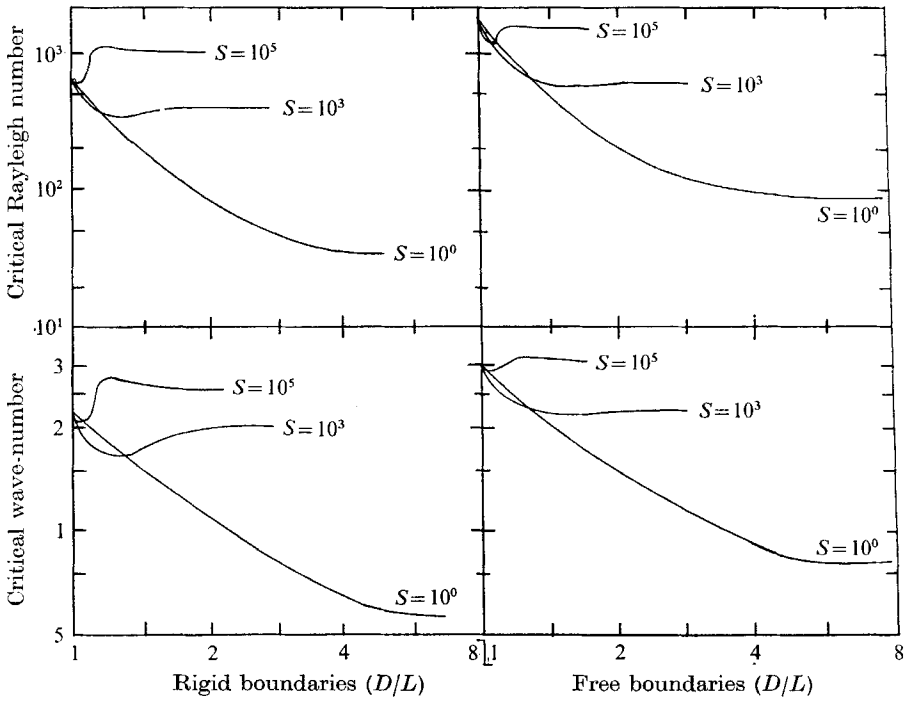

FIGURE 3. Predicted critical Rayleigh number and wave-number as functions of the depth ratio D/L for linear–linear profiles at various values of S.

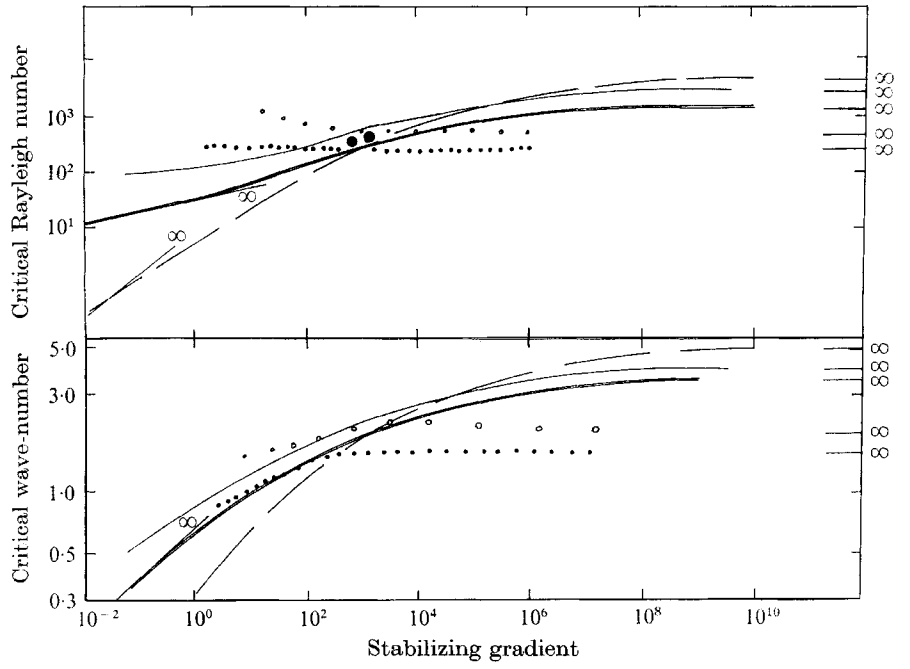

FIGURE 4. Critical Rayleigh number (top) and wave-number (bottom) of infinitely deep stable regions as functions of asymptotic dimensionless stable gradient S. =, linear–linear free; —, linear–linear rigid; — —, linear–antisymmetric; ..., exponential–linear free; oooo, exponential–linear rigid; ●, experimental results.

For the case of free-slip boundary at $z = 0$, the critical Rayleigh number approaches the $\frac{1}{4}$ power of S as a limit. This is in agreement with the calculations of Gribov & Gurevich. For non-slip boundary conditions the Rayleigh number has a much weaker dependence on S, decreasing to $S^{\frac{1}{30}}$ at $S = 0{\cdot}001$.

As $S \to \infty$. As S approaches ∞, the critical Rayleigh number approaches a constant. This can be anticipated, since the large stabilizing gradient prevents any effective penetration into the stable region. It is surprising, however, that the asymptotic values of Ra_c at large S are 2434·7 and 3487, for free-slip and non-slip boundaries respectively. These values are considerably greater than the free-rigid and rigid-rigid results for the classical Rayleigh–Bénard problem, indicating that a stratified layer of fluid may have greater stabilizing influences than a solid non-slip surface.

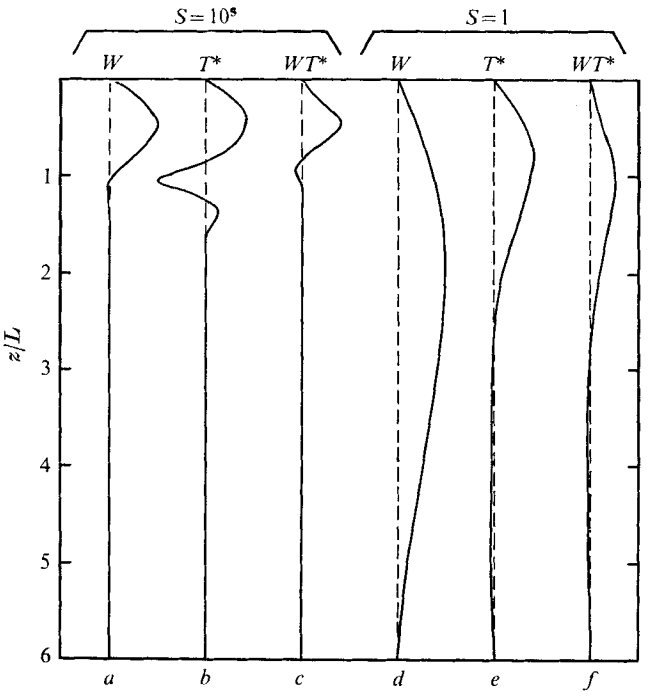

FIGURE 5. The velocity function W, a rescaled temperature T^*, and the product WT^* for the linear–linear profile with $S = 10^5$ and $S = 1$. Because this is a homogeneous problem, the absolute magnitude of W and T were arbitrary. Consequently, we let $W_{\max} = 1$, and to plot the temperature perturbation on a comparable scale we defined (*b*) $T^* = -2 \times 10^{-3}\, T$, (*c*) $T^* = -2 \times 10^{-3}\, T$, (*e*) $T^* = -10^{-1}\, T$, (*f*) $T^* = -10^{-1} T$.

This surprising result is perhaps better explained by examining the plot of WT^*, which represents the rate of work done by the buoyancy force. This is shown in figure 5. It is seen that while WT^* is positive in the major part of the flow field, there is a small region near the transition between the stable and unstable regions where WT^* is negative. In this plot, T^* is a rescaled temperature perturbation. Furthermore, as the depth of the stable region is increased, the depth of this negative region decreases while the magnitude of WT^* increases.

Consequently, the buoyancy force is always pumping energy into the stable region, resulting in a restraining mechanism for convection.

In Gribov & Gurevich (1957), the asymptotic free-slip boundary Ra_c for large S, was given as 370. This was traced to an error in their equations. A corrected derivation following their procedures yields an answer identical to the numerical results cited above.

Rintell (1967) calculated that as D/L increases, the minimum critical Rayleigh number should be 1100 when the stabilizing gradient is $1{\cdot}1 \times 10^{10}$. Figure 3 indicates how this result could be obtained. From our calculations, as D/L increases with a fixed S,† the critical Rayleigh number first decreases to a minimum, then increases. The decrease is less for greater values of S, and the minimum approaches the critical Rayleigh number when $D/L = 1$. Since Rintell's top boundary was free and the bottom boundary rigid, the calculated minimum critical Rayleigh number approaches the rigid-free value of 1100 for the Rayleigh–Bénard case as S becomes very large. Our results are consistent with Rintell's.

For the linear-antisymmetrical profiles, the results do not differ qualitatively from those found for linear–linear distributions, as seen in figure 4. When D/L is large and the stabilizing gradient low, critical Rayleigh number appears to be approaching the Gribov & Gurevich power law of $Ra_c = 7{\cdot}8S^{\frac{3}{4}}$. The wave-number, however, does not approach their power law of $a_c = 0{\cdot}6S^{\frac{1}{4}}$. When the stabilizing gradient is high, our results approach the value $Ra_c = 5866$, which greatly exceeds the limiting value of 107 predicted by Gribov & Gurevich. Wave-numbers also disagree markedly, being 5·07 in the limit for our case, and 2·6 for theirs.

The exponential–linear profile. The computed Ra_c and a_c for exponential–linear profiles (figure 2) are also shown in figure 4 as functions of S. It is indeed surprising to see that Ra_c is only weakly dependent on S. For the range of values considered, Ra_c is practically constant for the free-slip boundary case, and increased somewhat as S decreased for the non-slip boundary.

A more detailed examination of figures 2 and 4 indicates that this unexpected consequence is the result of two competing influences. In the first place, it is seen from figure 4 that the critical wave-number for the exponential–linear case behaves in a way quite similar to the linear–linear case. In both cases it decreases for decreasing S, due to the increased inherent depth scale of the stably stratified region. Corresponding to this decrease in wave-number or increase in cell size, there would be a tendency to reduce the critical Rayleigh number.

On the other hand, when S becomes progressively smaller, the destabilizing temperature difference becomes more and more concentrated in a narrow region near the top boundary, where W vanishes. This is illustrated in (2.24), where the exponential 'length scale' z_0 is less than L for small β. Therefore, the product $f(z)W$ becomes small everywhere, resulting in reduced power input to the fluid. This argument is substantiated by the computations of Sparrow *et al.* (1963), who found that for a shallow unstable layer Ra_c decreases when the temperature profile departs from the linear.

† Strictly speaking, Rintell did not fix S, but fixed $\chi = S/Ra_c$.

It is not surprising that the critical Rayleigh number associated with rigid boundaries increases at low S because the non-slip boundary conditions oppose a large value of W in just the region near the walls where the temperature difference is concentrated.

Parabolic profile. For infinitely large S, the exponential–linear profile approaches the parabolic profile, yielding

$$Ra_c = 275{\cdot}33,$$
$$a_c = 1{\cdot}58,$$

for a free boundary, in agreement with the calculation of Chandrasekhar (1961), and

$$Ra_c = 589{\cdot}44,$$
$$a_c = 2{\cdot}03,$$

for a non-slip boundary, in agreement with the calculation of Veronis (1963).

In summarizing the stability calculations, perhaps the most interesting conclusion which could be drawn is that an adjacent stably stratified region could represent a large energy sink, thus acting as a stabilizing agent for a thermally unstable fluid layer in increasing the critical Rayleigh number. While this effect is undoubtedly present in varying degrees for all temperature profiles, it is most apparent for the piecewise-linear profiles. Since the latter permit discontinuity in slope, it is possible to have extremely high stabilizing gradients immediately adjacent to the unstable layer. For other profiles with smooth transition between the stable and unstable regions, the effect is masked by other influences and clear-cut trends could not be easily observed in the experiment.

A similar difficulty exists for fluid layers bounded by regions of low stabilizing gradients. It is generally true that, as S becomes smaller, the flow field penetrates deeper into the stable regions, with the result that the critical wave-number tends to be smaller. For the piecewise-linear profiles, this results in reduced critical Rayleigh number. Again, for continuous profiles, as evidenced by the computations for the exponential–linear profiles, this effect is masked by other influences arising out of the complexity of the temperature distributions.

These difficulties in comparing different profiles are clearly due to the fact that the Rayleigh number, as it is usually defined, involves in fact only the parameters L and $\Delta\mathscr{t}$. Consequently, it is not an adequate indication of the stability of complex profiles, where the various depths have varying contributions to the stabilizing and destabilizing forces. The authors attempted a variety of algebraic definitions for the Rayleigh number, basing them upon physical arguments. None was found to be wholly satisfactory for all temperature distributions. One might expect that a definition based on certain integrals of the temperature profile would better describe the stability of such complex systems.

3. Structure and stability of supercritical flow

(i) *Experimental investigation of penetrative flows*

Many 'bathtub' examples of convection involve transient heating or cooling of a surface and penetration into a stable region; the 'soapy water' tessellated

polygons observed in 1882 by James Thompson could easily have arisen under such circumstances. Likewise, in nature there are bodies of fluids whose boundaries undergo daily or seasonal temperature variations—the surface of the ocean is a good example. Experimentally, models of these situations have been made by Foster (1965*b*) and Spangenberg & Rowland (1961) by changing the top surface temperature of an initially isothermal body of fluid. The problem differs from the one we propose to study in that flow in the isothermal region is resisted only by the relatively weak viscous forces, with the consequence that once convection commences the flow penetrates deep into the isothermal region and the entire system proceeds catastrophically to one of a completely different configuration. In the experiments of Spangenberg & Rowland and Foster evaporative cooling (approximating constant superficial heat flux) eventually restored the initial condition to a degree, and the process began a new cycle, to be repeated many times over. Such phenomena are not characteristic of systems with a stably stratified region, which resists the flow from the adjacent unstable region to an extent determined by the stable temperature gradient. Similarly the volume heating experiments of Tritton & Zarraga (1967) and Krishnamurti (1968*b*), though possessing curved temperature profiles, also were not concerned with stably stratified regions.

A similar experiment with a suddenly increasing bottom temperature produced convection which penetrated into an initially stratified fluid (see Deardorff, Willis & Lilly 1969). The stratification was not of a magnitude great enough to prevent penetration of the unstable fluid to the top of the tank, it merely could retard the rate of advance of the mixing.

The only thermal convection experiments with a stably stratified region of sufficient strength to limit the penetration of the fluid appears to be that of Townsend (1966) and some unpublished experiments of Furumoto & Rooth (see Veronis 1963). Both utilized water layers with the top and bottom boundary temperatures lying above and below 4 °C, which corresponds to maximum water density. While the scheme is indeed quite clever and the problem is also physically relevant to the formation of ice layers, the system appears to possess a unique mechanism of finite amplitude instability (Veronis 1963), which may not be shared by systems without such unusual density–temperature relationships. Furthermore, the density gradient in the stably stratified region could not be changed at will to investigate its effects on the flow.

In the present experiments, the required density profile was produced by maintaining a stable temperature gradient with controlled boundary temperatures, then providing radiative heating through the transparent boundary from the top. The radiative energy was absorbed and attenuated by the topmost layer of a few millimetres in depth, which then dissipated the heat by upward and downward heat conduction, resulting in a shallow unstable layer on top and a region of stable gradients below. The system could be maintained in a steady state, thus permitting the separation of purely transient effects from those which could persist for a long time. By changing the top and bottom boundary conditions in relation to the radiative heating power, the relative temperature gradient in the stable region could also be varied. In this manner the convection

at critical and supercritical Rayleigh numbers could be studied. The experiment thus showed results of a situation which is also hopefully tractable to theoretical expansion procedures about the marginal state. Questions about the form of convection in the two horizontal directions could be answered, as well as the nature of any subcritical finite amplitude instabilities. Lastly, details of the observed flows could be measured as a function of the experimental parameters to indicate the nature of the supercritical penetrative flows.

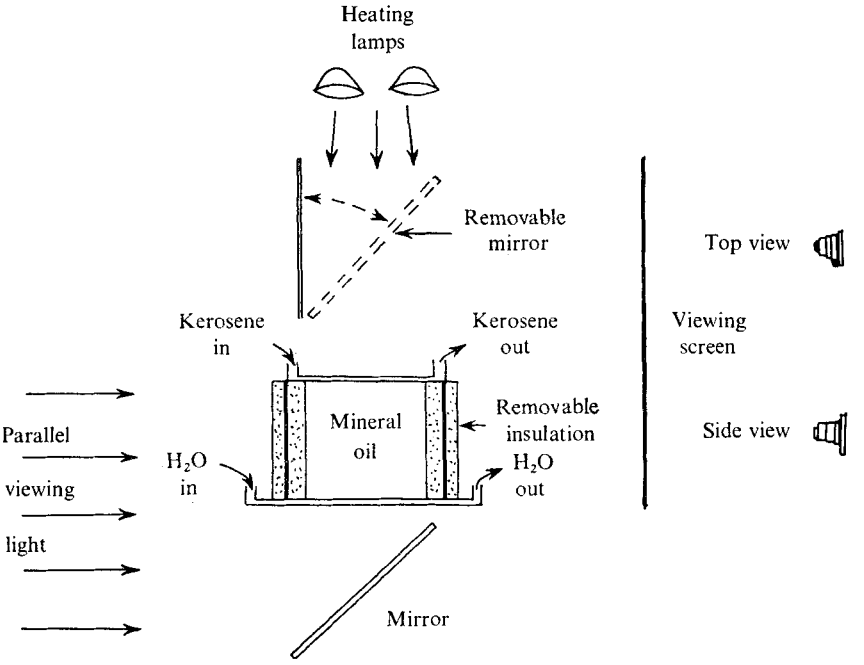

FIGURE 6. Schematic view of the experimental apparatus.

Apparatus. The apparatus shown in figure 6 consisted of a cubic glass tank one foot on each side. It was filled with mineral oil. The top and bottom surfaces were maintained at constant temperatures by circulating baths. Radiation from two 500-watt floodlights was introduced downward into the oil through the transparent top, and a substantial part of the energy from this radiation was absorbed by the top few centimetres of mineral oil, and subsequently lost through conduction and convection to the top surface. This resulted in a destabilized layer near the top in which convective currents originate. Visual observations were made using top-view and side-view shadowgraphs, while local temperature measurements were taken using a small movable thermocouple probe suspended on fine wires.

A number of steps were taken to ensure the precision and reproduceability of the experiments. Careful measurements of radiation as a function of depth in the oil enabled us to calculate the effective heat source and consequently the temperature distribution. The radiation was monitored periodically, and the variation in the input power was provided by a variable transmission rotating

chopper, so that the spectrum and hence the absorption characteristics of the light stayed constant from experiment to experiment. The two 500-watt quartz-iodine bulbs which supplied the heat energy had an estimated lifetime of 10,000 h and were measured to decrease by 4 % over the total 3500 h of the experiment.

Temperature (°C)	Viscosity (cp)
29·3	106
25·0	133
21·0	181
18·5	216
16·0	258
	Density (g/cm^3)
45·0	0·860
37·0	0·865
32·0	0·870
25·5	0·878
22·0	0·880
	Thermal conductivity cal/sec °C cm
22·0	0·00032
	Coefficient of expansion °C^{-1}
33·0	0·0011

Note: C_p was not measured but lies between 0·45 and 0·55 cal/g °C for most organic oils.

TABLE 1. Measured properties of the working fluid

It was necessary to take great care in eliminating horizontal inhomogeneities in the thermal field, as otherwise large-scale currents were easily set up in the tank. The two floodlights were situated 150 cm above the tank, the distance being a compromise between having uniform heating intensity up to five times that needed for instability (7·5 cal/sec over the 30 cm × 30 cm surface of the tank) with a variation in intensity of 5 % between the centre and the edge of the top of the tank, and a variation of 10 % between the centre and the corner of the top of the tank. The sidewalls were insulated by 2·5 cm of foamed polystyrene cemented to a copper plate which matched the stratified temperature gradient, the outside of which was covered with another 5·08 cm of foamed polystyrene. Only in this way was the thermal leakage out of the sides reduced to tolerable levels of 0·05 °C/cm, as compared to the vertical temperature gradients of 0·05 to 0·5 °C/cm.

The top coolant not only had to remove the heat from the convecting fluid below, but also was subjected to intense radiative heating from the lamps above. Consequently, relatively transparent Kerosene was chosen as the coolant, and the temperature drop of the fluid as it flowed through the $\frac{1}{4}$ in. plate glass bath was kept to below 0·5 °C by the rapidity of the Kerosene flow. The bottom coolant (water) did not have any substantial temperature drop as the radiative energy and temperature gradient was generally much smaller.

The working fluid was USP grade mineral oil, supplied by Dennison Laboratories, Providence, R.I. Its properties are given in table 1. The viscosity was measured with a Hoeppler viscosimeter for the various temperatures used. The density was measured as a function of temperature with a precision hydrometer good to 0·2 %. Thermal conductivity was measured at 25 °C in a hot wire thermoconductivity cell and was found to be 0·00032 cal/sec °C cm.

A thermal response time for this system is estimated as

$$t_0 = \frac{\rho C_p L_t^2}{k},$$

where ρ, k are given above.

L_t is one-half the length of the tank = 15 cm.

C_p is specific heat = 0·5 cal/g °C.

Using the above values, t_0 is found to be 27 h.

The bath temperatures were monitored at the inlet and outlet by thermometers and also by iron–constantin thermocouples. Since the principal aim was to observe steady experiments, no data was used if the thermometer readings varied by more than 0·1 °C over the course of an experiment. The temperature of the room was also kept to 25 ± 1 °C.

Details of the temperature structure in the convecting fluid were obtained using a thin uninsulated iron–constantin thermocouple of 0·065 mm diameter, the wire itself being 0·025 mm in diameter. It was stretched horizontally between two epoxy-insulated stainless steel vertical needles 2·5 cm apart, which projected up from a 0·25 cm horizontal stainless steel tube. The assembly could move both horizontally and vertically on a precise track, flat to 0·005 cm, and the position was monitored by two 10,000 ohm ten-turn variable resistors to an accuracy of 0·01 cm. The probe was moved in a horizontal direction to acquire data. This was done slowly enough so that the Reynolds number of the wire was less than 10^{-3} and was thus in the creeping flow or 'Stokes' flow régime. For such flows the speed of response of the probe would be governed more by the heat capacity of the surrounding fluid than by the thermal mass of the probe itself. Even assuming that all fluid within 10 probe diameters is actually 'dragged' by the probe, the thermal response time would still be better than 0·3 sec. The probe, scanning at 0·8 cm/sec would have a horizontal resolution of 0·24 cm. This is a conservative estimate. In reality the time constant could be as much as an order of magnitude faster than this.

The tank was made entirely of glass so parallel light could be projected through the tank to produce shadowgraph pictures of temperature inhomogeneities. A light source was placed with an arrangement of mirrors at an optical distance of 30 m. Side-view shadowgraphs were obtained by opening two hinged side insulators (see figure 6), and shining the nearly parallel light through the glass walls and on to a frosted plastic screen. In cases where it was felt that removing the insulation disturbed the convective flow too greatly, a limited view was obtained through two 7 cm × 10 cm double glassed windows on opposite sides. Top-view shadowgraphs were obtained by shining light upward through the bottom of the tank and projecting it with a removable mirror on to a frosted

plastic screen. Figure 6 shows the mirror arrangement. A Polaroid camera, a Bolex 16 mm movie camera, and a motor-driven 35 mm camera were mounted to record the shadowgraphs. The latter two cameras could be connected to a timer to obtain automatic sequencing in any interval from 10 sec to 30 min.

Procedure. Since only one working fluid was used, the only parameters capable of being varied experimentally were the total radiative power and the temperature difference between the top and bottom boundaries. The latter in essence fixes the asymptotic stabilizing temperature gradient, although in practice it is subject to a correction due to the radiative power input. In order to reveal physical trends, these two parameters must be varied systematically. The data presented below are discussed in terms of two systematic series of runs.

In series A the top to bottom temperature difference was held at several constant values while Q was varied from zero to 7·5 cal/sec. This was most convenient experimentally, but its results are difficult to interpret physically. To avoid uncertainties due to starting procedures, all runs were started after the system had been left at zero power for at least 10 h. Power was then turned on, and photographs and temperature scans were taken periodically.

In series B the temperature difference between top and bottom of the tank was kept proportional to heating power. In the absence of convection this leaves the shape of the unperturbed temperature distribution $\bar{\ell}(z)$ unchanged throughout the entire series, with the magnitude of $\bar{\ell}(z)$ being directly proportional to the intensity of the heating light and also the temperature difference between the top and bottom. Similarly L, the depth of the destabilized layer for a motionless fluid, remained constant. To reduce start-up time, the tests proceeded from one run to the next without returning to stagnant conditions.

(ii) *Experimental observations*

Critical Rayleigh number. The critical Rayleigh number can be experimentally determined by plotting the heating bulb power against $\Delta\bar{\ell}$ for various experimental runs, as shown in figure 7.

This was compared with the temperature difference calculated by measuring the intensity of light as it travelled down through the oil. The determined effective heat source was then fed into a finite difference computer program which calculated the value of $\Delta\bar{\ell}$ and L as a function of Q and β. The value of $\Delta\bar{\ell}$ at neutral stability was also determined. A sudden change in slope from this calculated (dashed) curve marks the appearance of convection. The comparison between the predicted curve and the experimental points in figure 8 and the data agrees to within a maximum estimated experimental error of $\pm 20\,\%$. The relation of these results to all the calculations is shown in figure 4.

Estimates for this error came from uncertainties in viscosity and thermal conductivity which consequently produced uncertainty about the precise depth of the temperature maximum for an undisturbed fluid. This resulted in an uncertainty in the coefficients used to predict the critical $\Delta\bar{\ell}$. However, in a given series of experiments the estimates of consistency of the data from point to point are much smaller, being less than $\pm 5\,\%$.

There was no hysteresis or other evidence of finite amplitude instability to

this value of $\pm 5\,\%$. The experimental points in figure 7 were not found in any particular order, and in some cases slightly subcritical experimental runs had a supercritical state as an initial condition. There was no evidence that the data from such runs differed from the data at the same point with an initial condition of no convection.

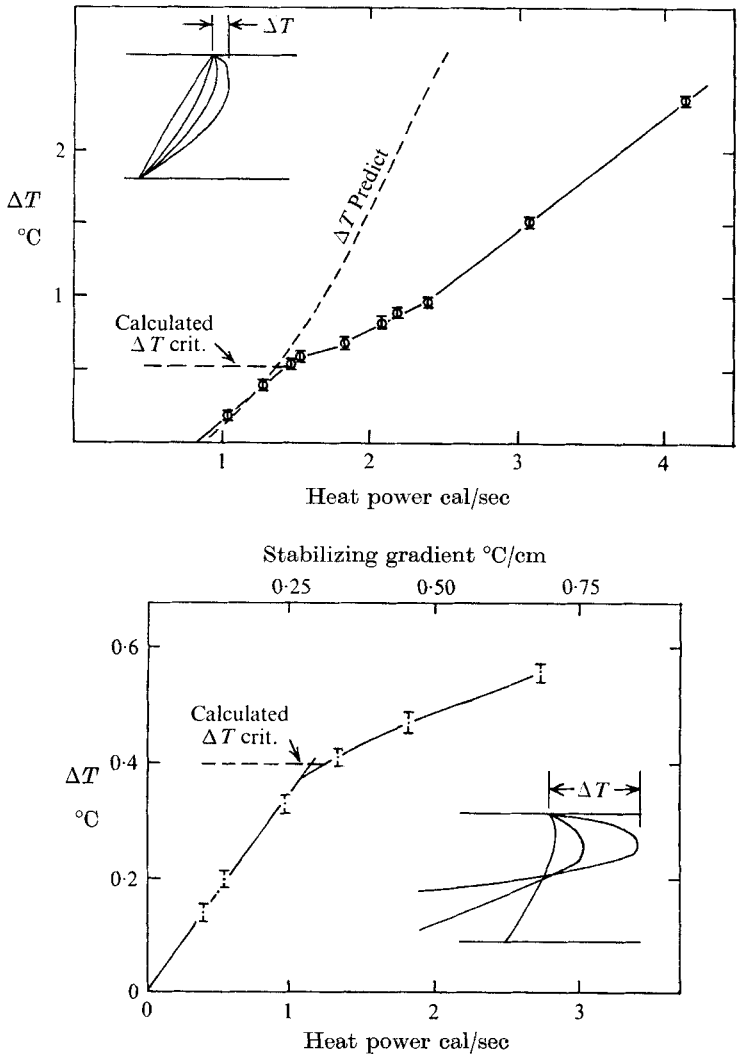

FIGURE 7. Experimental verification of onset. In the top figure calculated Ra_c was 564 with $S = 500$. In the bottom, calculated $Ra_c = 482$ with $S = 400$. These points are shown in figure 4 in relation to the calculations.

Visual observations of supercritical flows. From the pictures of shadowgraphs, figure 8 (plate 1), it can be seen that at supercritical conditions the motion consists of jets which plunge downward into the interior of the fluid. They appear as white dots when viewed by shadowgraph from above, and as white vertical lines when viewed by shadowgraph from the side.

The jets are intermittent in the sense that some jets tend to vanish after a period of time while others appear to take their place. Two neighbouring jets may also merge to form a single jet. This is shown in the circled regions in the sequence of pictures in figure 9 (plate 2). At first a white line connects the dots, indicating a falling sheet of fluid is forming. The line then becomes shorter as the jets grow closer together, until finally the original jets lose their identity, the line contracting to a single dot.

New jets first appear as an instability in the top thermal boundary layer. At a point between existing jets the boundary layer begins to thicken and bulge downward. The cool fluid within the bulge soon descends, appearing in a side view (see jet to the left of middle in figure 10 (plate 3)) as a rather large, cool blob. As the blob descends it is followed by cool fluid from the boundary layer which forms the jet. When the blob descends to a level where there is a stabilizing gradient, it slows considerably, vanishing to the surrounding fluid by heat conduction. Cool surface fluid continues to plunge in the jet which remains stable until it combines with a neighbouring jet.

Density of jets vs. *power*

If the jets had appeared in a regular periodic pattern, a well-defined wave-number could have been calculated from the observed distances between centres of the cells. In such a case the wave-number is uniquely related to the density of jets per unit area. Since the observed jets are clearly not periodic, it is only possible to present this type of observation in terms of jet densities.

A large number of jet counts were taken at various experimental parameters. This count must be viewed in a statistical manner, because intermittency of the jets causes their number to vary with time. The problems were reduced by averaging a large number of pictures. For the data presented, at least ten pictures spaced $1\frac{1}{2}$ min apart were counted. The counts were averaged, and a r.m.s. standard deviation was calculated. There was never a case when the standard deviation was more than 10 % of the mean value of dots in that series of pictures. In two cases enough photographs were counted (64) to obtain a Gaussian distribution, thus indicating that error was of the usual random nature.

Starting procedure for all series A runs exhibited the same sequence of behaviour. It is recalled that in series A all runs began with the same initial condition, i.e. there was a stable linear temperature distribution between top and bottom surfaces. After the heat lamp was turned on, the destabilized layer began to form on top, with convection beginning 1 to 5 h later. The jet density increased for the first few hours, reached a maximum, then decreased for the next 50 to 70 h before reaching steady state.

The steady-state measurements of jet density for both series of experiments are shown in figure 11. In general they increase significantly with heating light power. The jet density for series B appears to be directly proportional to heating bulb power. At the lower limit, both series should approach the values predicted from linear stability theory, although an ambiguity might exist due to the difficulty in assigning cell structures. For comparison, the number of hexagonal cell centres from linear stability theory is shown.

A crude measure of the depth to which convection can penetrate was found from horizontal temperature scans, such as figure 12, and was checked by side view shadowgraphs. It was found that in series B the penetration depth did not change significantly with heating power. Because of this, the width to depth ratio of the cells is inversely proportional to heating power in series B, and reaches a value of $\frac{1}{6}$ in the most extreme case observed.

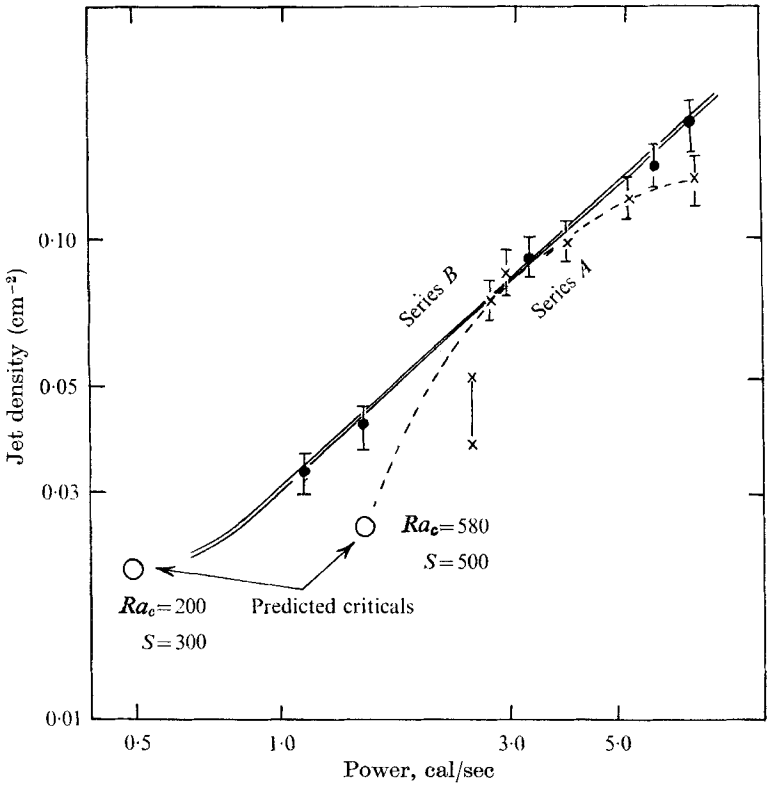

FIGURE 11. Steady jet density measurements.

Intermittency and average life time of the jets. A quantitative measure of the intermittency of the jet structure is the rate at which these jets appear and disappear. A careful accounting for one test at a power of 6·0 cal/sec (Ra = 5000) and a stable gradient of 0·91 °C/cm (S = 2020) showed that 14 jets appeared over a span of 5 min. Since there was a total of 56 jets in the viewing area, the average lifetime of a jet was 20 min. Less careful measurements at other power levels indicated that this rate of growth remained quite proportional to power for series B, and hence was inversely proportional to the square of the spacing between jets.

During one phase of the research it had been strongly suspected that the intermittency might be caused by large-scale motions due to inadvertent non-uniformities of the heat source or side boundary conditions. To check this an experiment was duplicated with extra precautions to ensure the uniformity of

the radiation flux. A more elaborate arrangement was also used to simulate the vertical temperature profile in the side walls, which consisted of a heating tape wrapped around the top of the sides of the tank to match both the destabilizing and stabilizing temperature gradients. Although these non-uniformities were decreased by more than an order of magnitude, the experiment resulted in an average lifetime for the jets of 20 min, identical to the above-mentioned measuret ment. The number of jets being swept into or out of the viewing area by large-scale motion in a period of 5 min was negligible (one). It was thus concluded that the intermittency was not due to large-scale circulation arising from non-uniform horizontal temperatures.

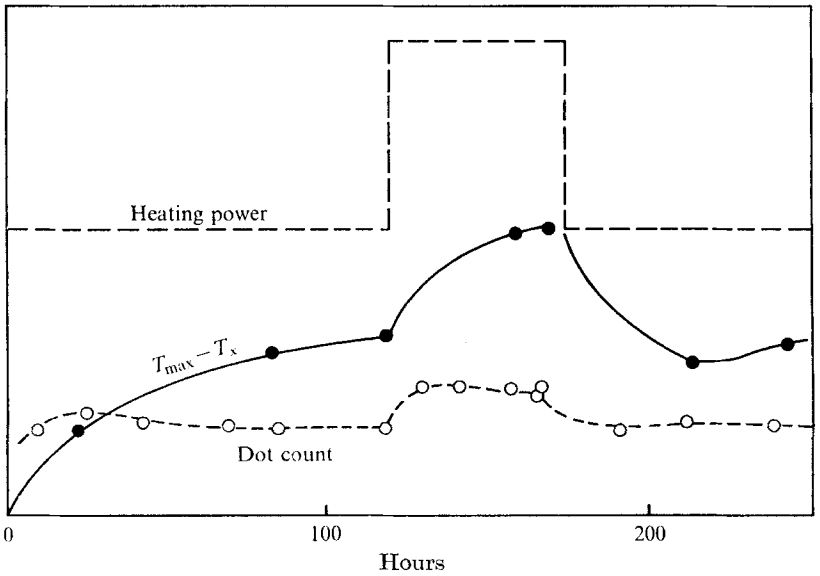

FIGURE 12. A transient study showing that parameters were independent of history.

Lack of history dependence. A long experiment was conducted to investigate the importance of history in determining the flow field and the parameters of the motion. The jet density was used as a measure of the state of the fluid, as shown in figure 12. The experiment began without radiant heating for 2 h. The heating lamp was then turned on and the attenuating chopper set at 2·5 cal/sec. The system was left for approximately 120 h in this state, with the mean number of jets being counted and the temperature distribution being measured. After 120 h, power was increased to 4·5 cal/sec. The apparatus was left for another 50 h, during which mean jet count and ΔT were found to change by 40 % and 50 % respectively. Radiant power was then reset to 2·5 cal/sec, and mean jet count and ΔT were observed to see if they returned to their previous values. After 100 h more, mean jet count was found to be only 4 % greater than the original count. The evolution of the maximum mean temperature and mean jet count are shown in figure 12. The system was seen to return to its original parameters, and it can be concluded that the value of these parameters is not determined by the history of the experiment.

No effort was made to use uniform starting procedure for the various series B experiments. The fact that data were consistent and reproducible was also an indication that the flow was not determined by the history of the experiment.

Recently Snyder (1969) reported that the number of rolls in a counter-rotating cylinder was strongly dependent on history. In his case, the flow has an adjacent stabilized region similar to the present studies. His flow was anisotropic in the form of steady periodically arranged two-dimensional rolls. Perhaps the intermittent motions observed in the present experiments were instrumental in keeping the jets free of any wall constraints by allowing continual adjustment of the flow structure. In a steady system the constraining effects of the side boundaries may be felt due to a lack of such an adjustment mechanism.

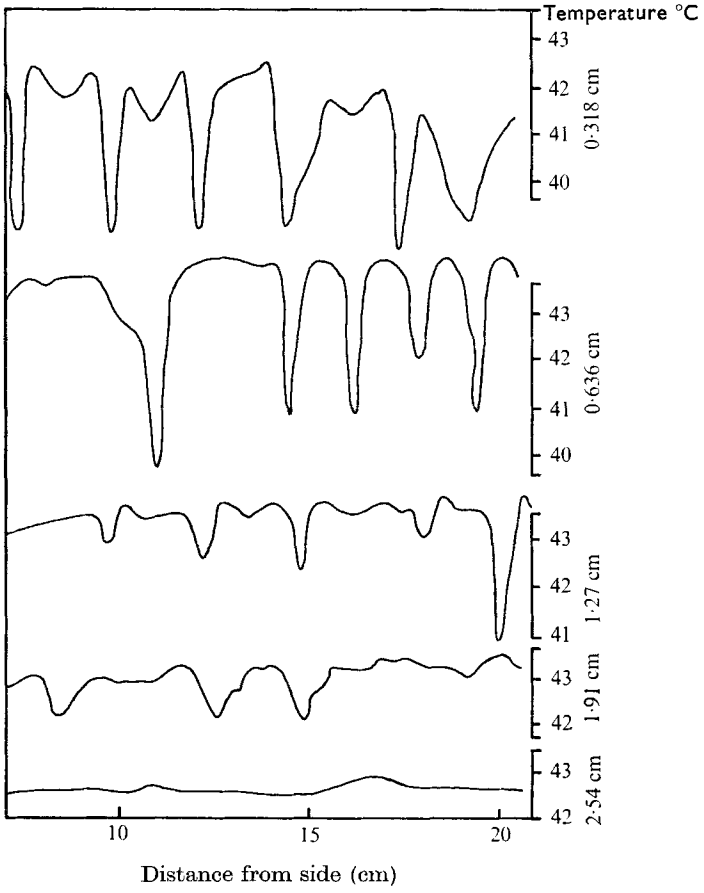

FIGURE 13. Typical temperature scans.

Structure of the cells. An idea of the structure of convective cells can be obtained from horizontal temperature scans by the movable thermocouple probe. A sequence of these scans at various depths below the top surface, such as those shown in figure 13, shows the width and amplitude of the cool descending jets.

When the amplitude of these jets was plotted against depth, as figure 14, it was noted that cool fluid heated up as it descended. It presumably absorbed heat from the hot upwelling fluid around it by thermal conduction.

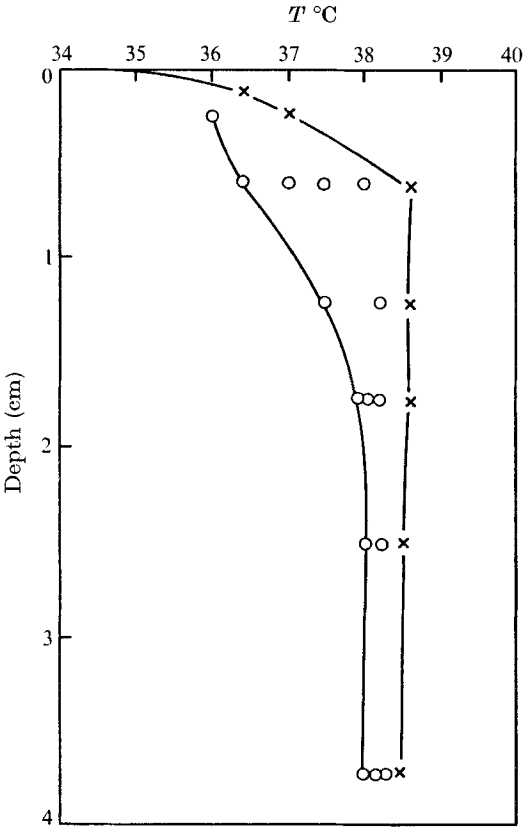

FIGURE 14. Amplitude of the jets as a function of depth.
○, peak jet temperature; ×, upwelling temperature.

Mushroom-like structure of jet fronts

An interesting aspect of the penetrative and intermittent motion is the mushroom-like structure associated with a few of the deep penetrating jets (see figure 8). Such structures have been associated with penetration into stratified fluid by Saunders (1962); in our case, they were more frequently observed with low stabilizing gradient where there was also more intermittent motion. A tentative explanation of their origin is given as follows. A new jet is formed when a blob of fluid becomes unstable. Time lapse movies and figure 10 show some blobs falling, and some of these apparently penetrate deeper than the steady jets. As a blob enters the stabilized region its velocity decreases rapidly, and it spreads out horizontally, acquiring the mushroom shape. The structure of these mushrooms is quite interesting, although to investigate it in more detail would involve considerable effort beyond the scope of the present studies.

Discussion of experimental observations. The various experimental investigations which have been made were generally exploratory in nature. In this spirit, only limited experimental data were obtained for the condition of marginal stability. To extend the range would require either changing the working fluid, which it was not possible to do without changing the optical absorption characteristics, or it would require using smaller stabilizing temperature gradients, which would increase interference from imperfect side wall conditions, and would result in a much larger margin of error.

However, in the limited range of parameters studied, an interesting finding of this experiment has been the absence of measurable subcritical finite-amplitude instability. As was said before, the expansions of Veronis (1963) and Krishnamurti (1968*a*) indicated that this instability should exist and be considerable, although the former had a rather unique finite-amplitude behaviour, and the latter was not necessarily valid for penetrative flows. In the present experiment, bulb power and stabilizing gradient were the independent variables. In series B runs, where unperturbed temperature amplitude is proportional to Q, there was no dip in the Q *vs.* ΔT curve which occurred in Krishnamurti's predictions. Spangenberg & Rowland (1961) noted that it took a much smaller Rayleigh number to sustain motion than to initiate it, almost by a factor of ten. This was not observed in our experiments.

The intermittent process observed in the rolls may be coupled to the inertial oscillations in the stabilized region which were reported by Townsend (1966). Aside from the intermittence of the jets, there was no other evidence of such oscillations in our case, probably because we were close to the marginal state and therefore inertia was negligible compared with viscous diffusion, whereas Townsend was considerably above the marginal state and so inertia was more important. In our experiment, the estimated period of inertial oscillations would range from 10 sec in the region of highest gradient to infinity in the isothermal region between the stable and unstable layers. The actual period would therefore be dependent upon the depth of penetration into the stabilized fluid; it is consequently amplitude-dependent, and a simple comparison is not possible.

One of the striking departures of these results, as well as the results of Tritton & Zarraga, from those of the classical Rayleigh–Bénard convection, was that the convection cells are not arranged in an orderly periodic structure, such as regular hexagons or two-dimensional rolls. On the other hand, the convective motion observed here is clearly not completely chaotic, as would be the case for complete turbulence. Thus, the observed flow structure has a measure of 'orderliness' lying somewhat between the complete regularity of Rayleigh–Bénard convection and true turbulent convection. This situation can be likened to the position occupied by liquid molecules in comparison with the ordered crystallinity of solids and the complete randomness of gas molecules.

In the case of uniform volume heating in a shallow tank without a stabilized region below, it has been shown theoretically by Krishnamurti (1968*a*) and Roberts (1967) that, if the temperature gradient decreases downward, the flow would consist of hexagons with cool fluid descending as a jet in the centre. In so far as our observed flow consisted of descending jets, it appeared to be in

partial agreement with their theories, although our observed structure lacked the regularity of hexagons. Their studies, of course, were not completely relevant to our problem, since their fluid layers were bounded by solid planes rather than stable regions. One is thus led to the speculation that the substitution of the solid boundary by a stably stratified region destroys the order which results in regular hexagons.

In contrast to the hexagonal observations is an experiment by Spangenberg & Rowland (1961) and Foster (1965*b*). They observed the transient and final motion of a water layer suddenly cooled from above by evaporation. A thick destabilized layer resulted from the evaporative cooling, and convective current was found to plunge into the isothermal liquid below. It is not clear whether evaporation over the entire surface was uniform, but the motion observed was not uniform. The observed flow was described as a series of intermittent plunging sheets and columns. Because of the free surface on top, each successive plunge could sweep all the cooled surface fluid with it into the interior, after which the motion stops because the destabilized layer has vanished. Eventually a new destabilized layer is generated by evaporation, and the cycle repeats itself. In contrast to our qualitative observations, Spangenberg & Rowland observed intermittent sheets of plunging liquid with only a few jets, whereas Foster observed predominantly jets.

In our experiments, the presence of the rigid top surface prevents the cold fluid from draining completely. Therefore, it is not obvious that the cause of the intermittency is the same as that suggested by Spangenberg & Rowland. On the other hand, the following sequence of events, proposed as a tentative explanation of the intermittency, bears some basic similarity to the mechanism of Spangenberg & Rowland. It appears that when pairs of jets are close together there is an instability with respect to their mutual distance, which arises because the total drag on the two jets would decrease, resulting in more efficient 'draining' and consequently drawing the jets even closer together. Eventually this process results in the two jets merging into one. This process serves to enhance mixing in the general area around these two jets, so that subsequently less temperature difference is available to act as a driving force. This results in temporarily inhibited convection. The process then repeats itself after a suitable period.

Our observation that cells came closer together as power was increased was a singular departure from observations of general convective flows (Chen & Whitehead 1968), and in particular from the observations of Tritton & Zarraga, where the cellular structure was observed to get very much wider as flow increased, up to five times the critical width. Our observations were quite consistent throughout all the experiments, and we feel strongly that they are valid for this experiment. Perhaps the absence of a solid boundary below the flow permits higher harmonics to enter into the flow pattern in a continuous manner, as opposed to the discrete manner in which Malkus (1954) suggested; and Krishnamurti (1968*c*, *d*) observed modes enter into the flow of fluids confined between two surfaces.

It must be remembered that the isothermal region remains constant, while the thermal boundary layer becomes shallower. It is reasonable to expect that the

driving force of the flow comes primarily from the thermal boundary layer, and that the unstable mode which results in jets is primarily related to the boundary-layer thickness. Consequently, the width-to-depth ratio of the cells becomes much smaller than unity.

This work was supported by National Science Foundation Grant GK-1702, and constituted part of the Ph.D. dissertation for one of the authors (J. A. W.) at Yale University.

REFERENCES

CHANDRASEKHAR, S. 1961 *Hydrodynamic and Hydromagnetic Stability*. Oxford University Press.

CHEN, M. M. & WHITEHEAD, J. A. 1968 Evolution of two-dimensional periodic Rayleigh convection cells of arbitrary wave-numbers. *J. Fluid Mech.* **31**, 1.

DEARDORFF, J. W., WILLIS, G. E. & LILLY, D. K. 1969 Laboratory investigation of non-steady penetrative convection. *J. Fluid Mech.* **35**, 7.

FOSTER, T. D. 1965*a* Stability of homogeneous fluid cooled uniformly from above. *Phys. Fluids*, **8**, 1249.

FOSTER, T. D. 1965*b* Onset of convection in a layer of fluid cooled from above. *Phys. Fluids*, **8**, 1770.

GRIBOV, V. N. & GUREVICH, L. E. 1957 On the theory of the stability of a layer located at a superadiabatic temperature gradient in a gravitational fluid. *J.E.T.P.* **4**, 720.

KRAUS, E. B. & ROOTH, C. 1961 Temperature and steady state vertical flux in the ocean surface layers. *Tellus*, **13**, 231.

KRISHNAMURTI, R. E. 1968*a* Finite amplitude convection with changing mean temperature. Part 1. Theory. *J. Fluid Mech.* **33**, 445.

KRISHNAMURTI, R. E. 1968*b* Finite amplitude convection with changing mean temperature. Part 2. An experimental test of theory. *J. Fluid Mech.* **33**, 457.

KRISHNAMURTI, R. E. 1968*c* On the transition to turbulent convection. Part I. Transition from two to three dimensional flow. *Geophysical Fluid Dynamics Institute Technical Report* 14. Florida State University.

KRISHNAMURTI, R. E. 1968*d* On the transition to turbulent convection. Part II. Transition to time-dependent flow. *Geophysical Fluid Dynamics Institute Technical Report* 16. Florida State University.

LEHNERT, B. 1967 Experimental evidence of plasma instabilities. *Plasma Physics*, **9**, 301.

MALKUS, W. V. R. 1954 Discrete transitions in turbulent convection. *Proc. Roy. Soc. Lond.* A **225**, 185.

MORTON, B. R. 1957 On the equilibrium of a stratified layer of fluid. *Quart. J. Mech. Appl. Math.* **10**, 433.

RINTELL, L. 1967 Penetrative convective instabilities. *Phys. Fluids*, **4**, 848.

ROBERTS, P. H. 1967 On non-linear Bénard convection. *J. Fluid Mech.* **30**, 33.

SAUNDERS, P. M. 1962 Penetrative convection in stably stratified fluids. *Tellus*, **14**, 177.

SEGEL, L. A. 1967 Non-linear hydrodynamic stability theory and its application to thermal convection and curved flows. *Non-Equilibrium Thermodynamics: Variational Techniques and Stability* (ed. R. J. Donnelly, L. Prigogine & R. Herman). University of Chicago Press.

SNYDER, H. A. 1969 Wave-number selection at finite amplitude in rotating Couette flow. *J. Fluid Mech.* **35**, 273.

SPANGENBERG, W. C. & ROWLAND, W. R. 1961 Convective circulation in water induced by evaporative cooling. *Phys. Fluids*, **4**, 743.

SPARROW, E. M., GOLDSTEIN, R. J. & JONSSON, V. K. 1963 Thermal instability in a horizontal fluid layer, the effect of boundary conditions and non-linear temperature profile. *J. Fluid Mech.* **18**, 513.

THOMPSON, J. J. 1882 On a changing tesselated structure in certain liquids. *Proc. Glasgow Phil. Soc.* **13**, 464.

TOWNSEND, A. A. 1966 Natural convection in water over an ice surface. *Quart. J. Roy. Met. Soc.* **90**, 248.

TRITTON, D. J. & ZARRAGA, M. N. 1967 Convection in horizontal layers with interna heat generation. *J. Fluid Mech.* **30**, 21.

VERONIS, G. 1963 Penetrative convection. *Astrophysical J.* **137**, 641.

WHITEHEAD, J. A. 1968 Stability and convection of a thermally destabilized layer of fluid above a stabilized region. Ph.D. Thesis, Yale University.

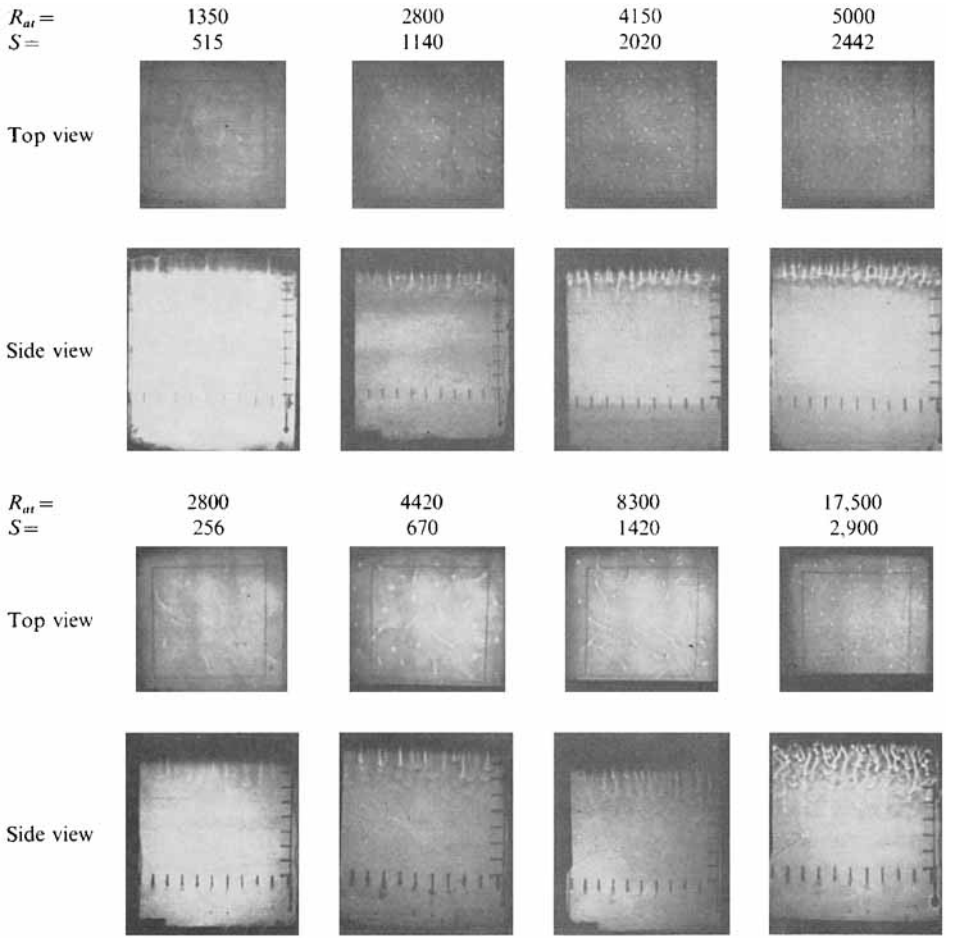

FIGURE 8. Top and side shadowgraph views of the convective motion.

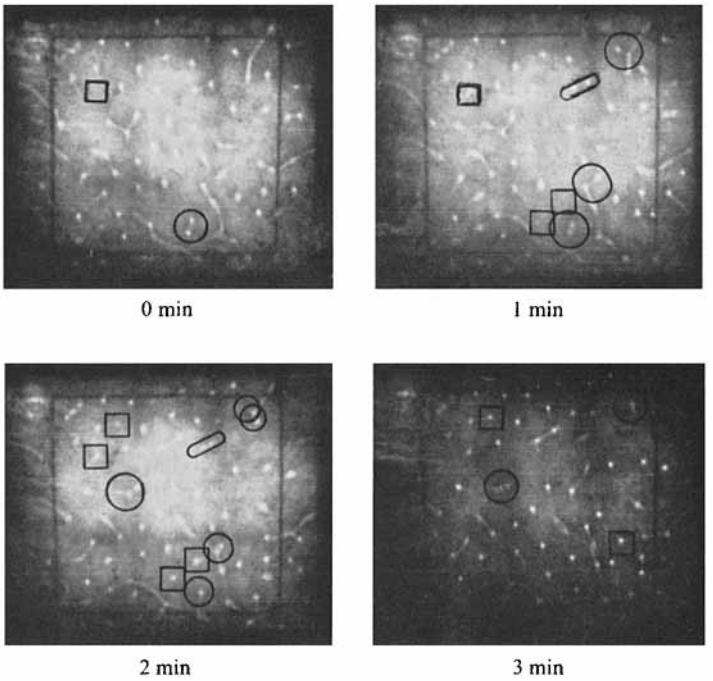

FIGURE 9. Time sequence of a top shadowgraph picture showing non-stationary behaviour of jets. The sequences of circles show neighbouring jets (white dots) as they merge, while the sequences of squares show new jets forming to fill the gaps.

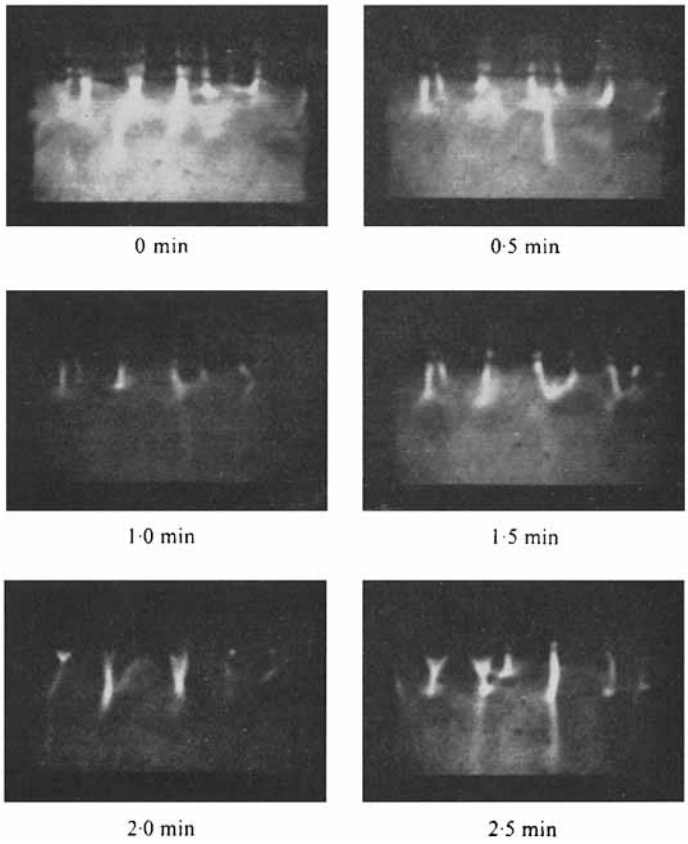

FIGURE 10. Time sequence of side shadowgraph pictures showing the formation of a new jet and merging of neighbouring jets. The dark upper portion of the picture is greatly stretched in the vertical direction due to the top temperature gradient.